Limnology and Oceanography
FLUIDS & ENVIRONMENTS

ORIGINAL ARTICLE

Vegetation wakes and wake interaction shaping aquatic landscape evolution

John M. Kondziolka and Heidi M. Nepf

Abstract

*Recent field and experimental studies show that the wakes behind individual patches of aquatic vegetation, as well as the interaction and merger of neighboring wakes, produce zones of diminished velocity that may enhance deposition and encourage patch growth and patch merger. In the present study, these patch-scale biogeomorphic interactions are incorporated into a simple model for vegetated landscape evolution. The initial flow field is solved by using a porous media formulation for hydraulic resistance. The velocity in wake regions is then adjusted to match the wake structure measured in laboratory studies with individual and pairs of vegetation patches. Vegetation is added based on a probabilistic function linked to the velocity field. The simulations explore the influence of initial plant density (*ID*) and limiting velocity (*LV*, the velocity above which no plants can grow) on landscape evolution. Three types of stable landforms can occur: full vegetation coverage, channeled, and sparse. By including the influence of wakes, full vegetation coverage can be achieved from initial plant densities as low as 5%. In contrast, simulations that exclude the influence of wakes rarely reach full vegetation coverage, reinforcing the idea that growth within wakes is an important component in vegetated landscape evolution. The model also highlights the role of flow diversion into bare regions (channels) in the promotion of growth within vegetated regions. Finally, sparse landscapes result when the initial plant density is sufficiently low that no wake interactions can occur, so that patch merger cannot occur, emphasizing the importance of the patch interaction length scale.*

Keywords: biogeomorphic feedbacks, model, ecosystem, restoration

Introduction

[1] Mangroves, seagrasses, and coastal marshes are important for their inherent value as habitats (van Katwijk et al. 2009), their benefit in protecting sediment from erosion (Wolters et al. 2005), and their high capacity as carbon sinks (Duke et al. 2007). Continued loss of these aquatic environments has accelerated the need for their restoration (Wolters et al. 2005; van Katwijk et al. 2009; Orth et al. 2010). Understanding the interaction between flow and vegetation could improve plans for both restoration and development in vegetated ecosystems and built environments near waterways (Marani et al. 2006; Larsen and Harvey 2011; Bentley and Karunarathna 2012). For example, van Katwijk et al. (2009) note that plant–flow feedbacks can influence the optimum transplantation techniques for restoration. In particular, they suggest that increasing the planting density and/or planted area provides a greater benefit to restoration success in exposed areas than in

Department of Civil and Environmental Engineering, Massachusetts Institute of Technology, Cambridge, Massachusetts 02139, USA

Correspondence to John Kondziolka, kondzi@mit.edu

sheltered areas. This is because in exposed areas, where the current speeds are higher, vegetation creates a larger reduction in local velocity, with the magnitude of reduction linked to planting density and size.

[2] The dynamic interactions among flow, sediment, and vegetation have been explored in several research studies. At the landscape scale, vegetation feedbacks have been examined using computer models. For example, Mariotti and Fagherazzi (2010) used a one-dimensional numerical model of sediment transport to analyze long-term evolution of salt marshes under the effects of sea level rise. They noted that vegetation plays an important role by physically trapping sediment and dissipating waves, and their model incorporated these vegetation–sediment feedbacks by correlating erodibility to aboveground biomass and by increasing the sedimentation rate in vegetated areas. Larsen and Harvey (2011) developed a cellular automata model incorporating the effect of vegetative flow resistance into a sediment transport scheme that produced many different types of realistic landforms. Vegetation in the model altered a porosity term that represented the hydrodynamic resistance and also modified the eddy viscosities in the longitudinal and transverse directions.

[3] Other studies have linked flow, deposition, and the spatial development of vegetation at the scale of individual patches and islands. For example, the wakes behind individual patches of vegetation and woody debris have been shown to create regions of elevated fine-particle deposition that promote vegetation growth and the subsequent elongation of the patch (see, e.g., Gurnell et al. 2001; Gurnell et al. 2008; and Chen et al. 2012). The area of fine-particle deposition is associated with a region of reduced velocity and turbulence that extends a distance L_1 downstream from the patch. Zong and Nepf (2011) showed that L_1 can be predicted from the patch diameter and stem density. In contrast, the region of flow acceleration adjacent to a patch inhibits plant growth. For example, using transplantation of real plants in a river, van Wesenbeeck et al. (2008) showed that placing a new patch adjacent to and within the range of influence of an existing patch, which was 0.5 m for a 1-m-diameter patch, had a significant negative effect on the biomass development of the new patch.

[4] More recently, Vandenbruwaene et al. (2011) further explored the effect of neighboring patches and concluded that flow acceleration, which they observed between adjacent patches, would promote erosion, which would inhibit patch merger. However, Meire et al. (2014) drew a different conclusion by observing the flow and deposition field over a larger spatial scale than Vandenbruwaene et al. (2011). Specifically, Meire et al. (2014) suggested that patch merger is possible under some conditions because the interaction of wakes formed by the individual patches produced a region of depressed velocity and enhanced deposition on the centerline between neighboring patches, but at a distance (L_m) downstream of the patches (secondary deposition zone in Fig. 1). The distance L_m increases with increasing patch diameter (D) and gap width (Δ), and decreases with increasing patch solid volume faction (φ). Meire at al. (2014) showed that the length of

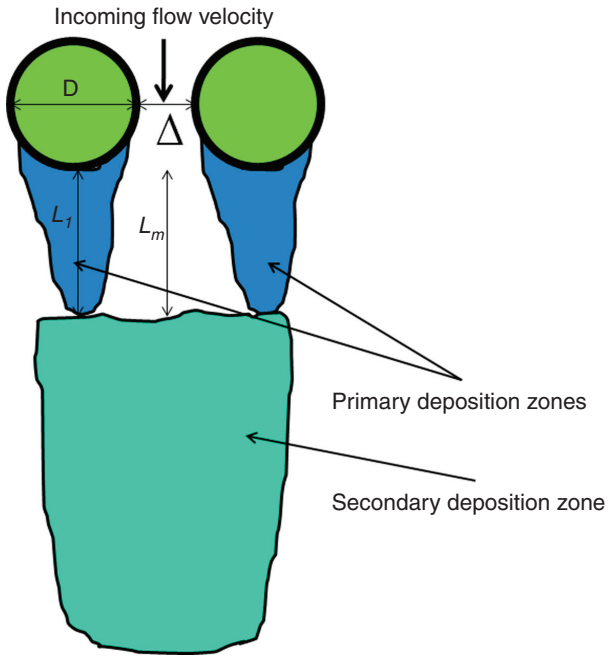

Fig. 1 Diagram illustrating the effect of local hydrodynamics on deposition downstream of a pair of vegetation patches, based on Meire et al. (2014). Flow is from top to bottom. Patches of vegetation are shown as thick green circles and are separated by a gap width Δ. The primary deposition zones (shaded blue) immediately downstream of each patch extend a distance L_1 from the back of the patches, as studied in Zong and Nepf (2011). A region of secondary deposition (blue green) is present further downstream of the two patches, beginning at approximately L_m from the patches. In the scenario shown, L_1 and L_m are close enough that the primary and secondary regions of deposition are connected.

the primary deposition zone (L_1) is not impacted by the presence of a neighboring patch. Further, at small gap widths (Δ) the primary and secondary deposition zones merge, as shown in Fig. 1. Because previous studies have linked sites of deposition to areas of vegetation growth (Gurnell et al. 2005; van Wesenbeeck et al. 2008), Meire et al. (2014) theorized that the zones of deposition would become filled with vegetation over time, and the new vegetation would eventually block flow on the centerline, leading to a merger of the original patches into a larger vegetated structure.

[5] The goals of this study are to incorporate the flow–biogeomorphic interactions at the patch scale shown in Fig. 1 into a simple model for vegetation development and to evaluate their importance to landscape evolution. The model simulates landscape evolution over 5–300 cycles of vegetation growth, and the model outcomes are related to real landscape patterns and field studies of restoration efforts.

Methods

[6] The simulation was initialized by populating the domain with vegetation patches at a random set of locations. The number of patches was chosen to achieve a preselected value of initial area density (*ID*). Using the initial distribution of vegetation, we solved for the velocity field. Based on the velocity field, new vegetation was added, which changed the velocity field in the next computed step. The process was repeated until the simulation converged to a stable state.

[7] The model was coded in Matlab (version 8.2, Mathworks, Natick, Mass., USA) and utilized the groundwater modeling software MODFLOW-2005 (version 1.1100; U.S. Geological Survey, USA) as an efficient numerical solver for the steady-velocity field associated with a prescribed hydraulic head difference and distribution of flow resistance, represented by permeability within MODFLOW. The model represents systems driven by a spatial gradient in water surface elevation (dH/dx, where H is the hydraulic head and x is the distance), as is the case for many coastal environments and wetlands. The model directly represents unidirectional flow, such as the conditions studied in Vandenbruwaene et al. (2011) and Meire et al. (2014). It is also a useful simplification to the complex flow fields encountered in coastal environments. Although tidal currents may change direction as well as magnitude over the course of a tidal cycle, peak currents typically have a consistent direction, so that the effect on erosion and deposition near vegetation may be correlated with a particular current direction, for example, as observed in the field for individual patches (Bouma et al. 2007) and at a larger scale in the evolution of a *Spartina anglica* marsh (Temmerman et al. 2007).

[8] Following Lowe et al. (2008), we drew an analogy to porous media and defined a linear drag law with drag coefficient C_d, which can be related to an effective permeability $K = g/C_d$, with gravitational acceleration g. Assuming steady flow, the depth-averaged velocity field (U, V) in the coordinate directions (x,y), respectively, is described by the conservation of momentum,

$$U\frac{\partial U}{\partial x} + V\frac{\partial U}{\partial y} = -g\frac{\partial H}{\partial x} - C_d U + \nu_t\left(\frac{\partial^2 U}{\partial x^2} + \frac{\partial^2 U}{\partial y^2}\right), \quad (1)$$

$$U\frac{\partial V}{\partial x} + V\frac{\partial V}{\partial y} = -g\frac{\partial H}{\partial y} - C_d V + \nu_t\left(\frac{\partial^2 V}{\partial x^2} + \frac{\partial^2 V}{\partial y^2}\right) \quad (2)$$

with eddy viscosity ν_t. To utilize the rapid computational advantage of MODFLOW, we simplified Eqs. (1) and (2) with the assumption that throughout most of the flow domain the inertial and shear-stress terms were small compared with the drag terms. Then, substituting the effective permeability $K = g/C_d$, (1) and (2) can be reduced to

$$U = -K\frac{\partial H}{\partial x}, \quad (3)$$

$$V = -K\frac{\partial H}{\partial y}. \quad (4)$$

Combining with continuity,

$$\frac{\partial}{\partial x}K\frac{\partial H}{\partial x} + \frac{\partial}{\partial y}K\frac{\partial H}{\partial y} = 0 \quad (5)$$

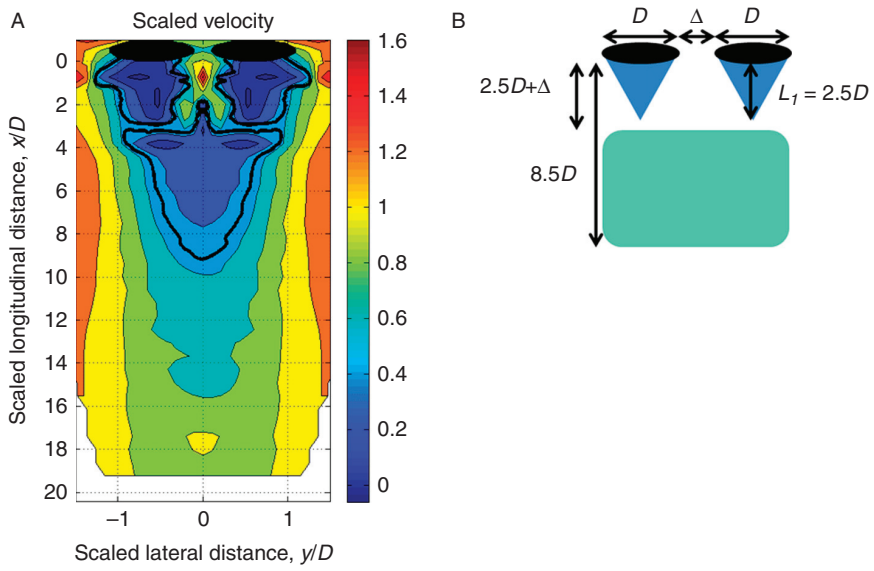

Fig. 2 A — Measured velocity field around two patches (D = 22 cm, φ = 10%, Δ/D = 0.1) scaled by the upstream, incoming velocity, U_0 from Meire et al. (2014). The longitudinal and lateral distances are scaled by the patch diameter. The position and extent of the mimic vegetation is shown with black shading. Measurements made over the span y/D = 0 to 1 are reflected over the y = 0 axis, based on expected symmetry. The heavier contour marks the isovel $0.5U_0$. B — A diagram of the wake modifications made to the velocity field after each MODFLOW calculation. The near wake zone extends a distance $L_1 = 2.5D$ from each patch (shown in blue). In this zone the velocity was reduced to 20% of the MODFLOW calculated value. Within the secondary deposition zone (shown in blue green) the velocity was reduced to 50% of the local MODFLOW value. The length of the merged wake (blue green) is chosen to match the zone defined by the $0.5U_0$ isovel in (A).

MODFLOW (Harbaugh 2005) solved Eq. (5), producing the distribution of water elevation $H(x,y)$, from which the velocity fields (U, V) were extracted using Eqs. (3) and (4). In the wakes of vegetation patches, the shear (e.g., $\nu_t\ \partial^2 U/\partial y^2$) and inertial (e.g., $U\partial U/\partial x$) terms can be important, and we added back these effects by using the experimental observations of Zong and Nepf (2011), Chen et al. (2012), and Meire et al. (2014). This method, which uses MODFLOW to solve the drag-dominated flow field and manually adjusts for patch wakes, was chosen to facilitate rapid simulations compared with full hydrodynamic models.

[9] The values for effective permeability, K, were estimated by comparing model runs with experimental measurements. Flow around a circular, emergent patch of vegetation was modeled in MODFLOW by assigning the circular region a lower permeability than the background (unvegetated) region and applying a head difference between the upstream and downstream boundary, while setting the lateral flow at the side boundaries far away from the patch to be zero. The permeability of the vegetated region was adjusted until the exit velocity from the patch matched measured values for the target case, a patch of diameter D = 22 cm and φ = 10% (see figure 7 in Chen et al. 2012). For the prescribed head gradient of 0.001, the best fit was achieved with permeabilities of 310 m d^{-1} and 31 m d^{-1} in the bare and vegetated regions, respectively. The same head difference and calibrated permeability were used in all subsequent simulations.

[10] The wake correction to the velocity field was formulated based on measurements from several studies. A diagram of the modifications is shown in Fig. 2, alongside experimental data for a neighboring patch case (Meire et al. 2014). Zong and Nepf (2011) found that a region of depressed velocity exists immediately downstream of a single patch and that deposition is enhanced within this region. Moreover, Follett and Nepf (2012) observed this zone to be triangular in shape (as shown in Fig. 1), consistent with the idea of linear shear layer growth. For the stem density considered here, L_1 = 2.5D (Zong and Nepf 2011). Meire et al. (2014) showed that neighboring patches do not alter the length-scale L_1, so that this value is applicable for any patch spacing. Further, Meire et al. (2014) showed that within this triangular region the velocity is depressed to ~20% of the magnitude upstream of the patch. To mimic this behavior in our model, the velocity was reduced to 20% of the MODFLOW value in this region. Meire et al. (2014) also showed that a second region of depressed velocity occurs on the centerline between two patches from the interaction of the individual patch wakes. Unlike L_1, the distance to the beginning of the secondary zone of diminished velocity, L_m, has some dependence on gap spacing (Δ). For simplicity, we used the value L_m

$= L_1 + \Delta$. When two patches were within 1 diameter of each other, a secondary region of diminished velocity was imposed between $L_m = 2.5D + \Delta$ and $8.5D$ behind the patches (shown as the light green zone in Fig. 2B). The length of this zone was chosen to capture, in a simplified manner, the region within which velocity was reduced by $\geq$50%. This region is highlighted in Fig. 2A by the thicker contour at the $0.5U_0$ isovel. For simplicity, patches with gap width larger than one patch diameter were assumed to have no secondary interaction. For the case shown in Fig. 2 the region of diminished velocity extends over $8.5D$ behind the patch pair. For comparison, in the original velocity field calculated by MODFLOW, reduced velocity extends only $1.5D$ behind each patch.

[11] As noted above, previous studies have linked vegetation growth to areas of enhanced deposition (Scott et al. 1996; Gurnell et al. 2001), and areas of enhanced deposition have been linked to regions of reduced velocity (Sand-Jensen 1998; Chen et al. 2012; Schoelynck et al. 2012). In addition, vegetation within regions of reduced velocity is less prone to dislodgement. Conversely, elevated velocity, especially above the threshold for sediment motion, may dislodge seedlings and inhibit vegetation growth (Luhar et al. 2008; van Wesenbeeck et al. 2008; Bouma et al. 2009). Based on these observed relationships, vegetation addition in the proposed model was linked to the velocity field by using the following procedure. All velocities were scaled by the bare-bed velocity, U_0, that is, the velocity with no vegetation present. At a scaled velocity of 1, when the local velocity was equal to the bare-bed velocity, the probability of vegetation occurrence was set to 0. At a scaled velocity of 0, the probability of vegetation was set to 1. A linear relationship was chosen between these two limits, as illustrated in Fig. 3, similar to that described by Couwenberg (2005). Note that the form of the vegetation addition curve assumes that the main limiting factors for growth are hydrodynamic stress, sediment motion, and resuspension. It excludes scenarios in which growth is limited by factors other than current speed, such as disease or high turbidity not associated with resuspension. Additionally, we define a limiting velocity (*LV*) above which no vegetation additions are possible; that is, the probability of vegetation drops to zero for velocity above *LV*, as shown by the vertical line deviating from the linear pattern in Fig. 3. Conceptually, the limiting velocity could be associated with significant sediment motion, which inhibits vegetation growth because seedlings have difficulty taking root and resuspension of fine material may reduce light availability. Although light availability and dislodgement affect plants regardless of reproductive mechanism, the conceptual model for high velocity inhibiting seed deposition and seedling rooting may make the model more suitable for application to plants spread by seeds or propagules. Note that *LV* is defined relative to the bare-bed velocity (U_0). For example, a high value of *LV* corresponds to a region for which the velocity only needs to be slightly depressed below the bare-bed conditions (U_0) for growth to occur. A low value of *LV* corresponds to a region for which the velocity must be depressed significantly below U_0 before growth can occur.

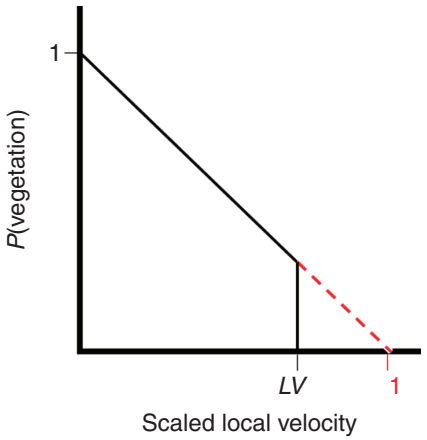

Fig. 3 Probability distribution governing the likelihood of vegetation as a function of the scaled velocity. The scaled velocity is the ratio of the local velocity with vegetation to the velocity observed when no vegetation is present (U_0). The probability of growth is 100% (1) for zero velocity and declines linearly to zero for local velocity equal to the bare-bed velocity, that is, a scaled velocity of 1. In addition, each run is assigned a limiting velocity (*LV*), defining the velocity above which no vegetation additions are possible.

[12] Simulations of landscape evolution were run on a grid of 500 by 500 cells. Pioneer vegetation was initially established randomly throughout the grid in square patches of 3 by 3 cells by selecting a random grid cell as the center of a patch and assigning it, along with the eight surrounding cells, the vegetation

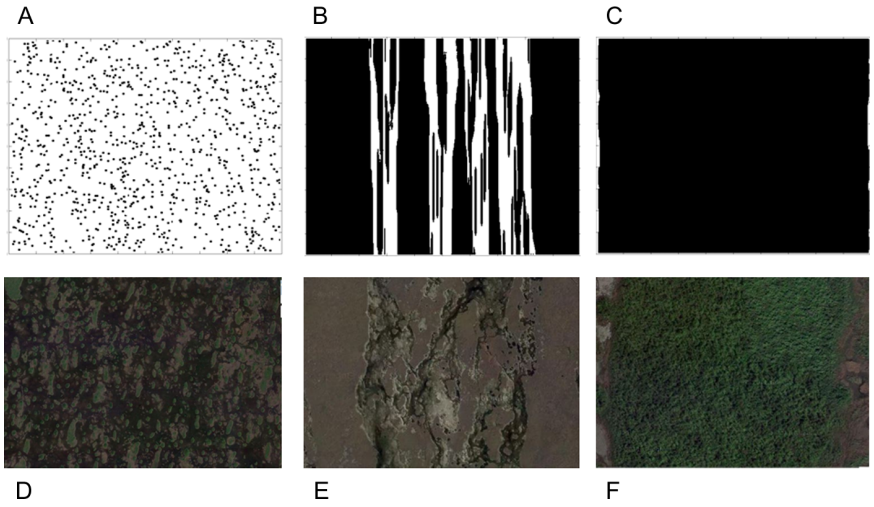

Fig. 4 Examples of (A) sparse, (B) channeled, and (C) filled end-states produced by the landscape simulation. *ID* is the initial density of the simulation, and *LV* defines the limiting velocity above which no vegetation additions are possible. *ID* = 4% for each case, with *LV* = 0, 0.1, and 0.7, respectively. The sparse case has a low final density equal or near to its starting value. The channeled case has a final density between 40% and 90% and visually shows a channel pattern with vegetation extending from the top to the bottom of the flow domain. The filled case exhibits a final density near 100%. Below, examples from the Florida Everglades of landscapes visually classified as (D) sparse, (E) channeled, and (F) filled by using satellite data available from Google Earth.

permeability. Setting the initial patch size to 9 grid cells allows the model to resolve vegetation additions at scales less than the diameter of the patch. All other grid cells were assigned the unvegetated permeability. The velocity field was calculated in MODFLOW, modified to account for wakes, and then evaluated for vegetation development by using the probabilistic rules shown in Fig. 3. A random number between 0 and 1 was selected in Matlab. The mean value of the distribution, 0.5, was subtracted, and then the probability of vegetation within the cell (based on the scaled velocity in that cell) was added directly to that value. The result was rounded to the nearest integer, leading to a binary matrix of cells in vegetated and unvegetated states. In addition, all cells with velocity above *LV* were left unvegetated. The first and last four rows and columns of the grid were kept free of vegetation to prevent the boundary from affecting the evolution. After one cycle of probabilistic vegetation additions, a new velocity field was computed, and the process was repeated. This continued until the vegetation growth effectively stopped, defined by the constraint that over three consecutive time-steps the total area density changed by $<0.5\%$. This constraint prevented any one time-step's probabilistic variation from prematurely terminating the simulation and saved time by preventing incremental changes in density from continuing the simulation indefinitely. Both the velocity field and the vegetation distribution were saved at each time-step.

[13] Two free parameters were modified between cases: the limiting velocity (*LV*) above which no vegetation additions were allowed, and the initial density (*ID*) of vegetation. *LV* was varied between 0 and 1, and *ID* was varied between 0.01% and 96%. By varying these two parameters, a variety of steady-state landscape patterns were produced that mimicked patterns found in nature. To evaluate the importance of patch-scale interaction, the simulations were also run without the wake modification to the velocity field.

Results

[14] The final, stable landscapes produced by the simulations can be broadly categorized into three types: sparse, channeled, and filled (100% coverage), which correspond to landscapes observed in the field (Fig. 4). The sparse cases generally occurred at low *ID* or low *LV*, the filled cases occurred at high *ID* or high *LV*, and the channeled cases occurred at the boundary between sparse and filled cases, as shown in Fig. 5. Values for simulations that were run to completion have letters in bold and underlined, whereas plain letters represent reasonable predictions based on computed conditions. For example, if *ID* = 0.9%, *LV* = 0.6 had a sparse outcome, then *ID* = 0.9%, *LV* = 0.5 also had a sparse outcome because the tendency for growth declines with decreasing *LV* because the velocity must be depressed to a greater degree to facilitate growth (Fig. 3). Similarly, because *ID* = 3.3%, *LV* = 0.6 produced a filled

ID \ *LV*	0	0.05	0.1	0.2	0.3	0.4	0.5	0.6	0.7	0.8	0.9	1
0.07	S	S	S	S	S	**S**	S	S	S	S	**C**	F
0.09	S	S	S	S	S	S	S	**S**	S	S	**C**	F
0.4	S	S	**S**	S	S	**S**	S	**S**	**S**	**C**	F	F
0.9	S	S	**S**	**S**	S	**S**	S	**S**	**C**	**C**	**F**	F
1.8	S	**S**	**S**	**C**	C	**C**	C	**C**	C	**C**	F	F
3.3	S	**C**	**C**	C	**C**	**C**	**C**	**F**	F	F	F	F
3.5	S	C	C	**C**	**C**	**F**	F	**F**	F	**F**	F	F
4.3	S	**C**	**F**	**F**	F	**F**	F	**F**	F	**F**	F	F
5.2	S	**F**	F	F	F	F	F	F	F	F	F	F
6	S	F	**F**	**F**	F	**F**	F	F	F	F	F	F

Fig. 5 Summary of the simulation outcomes at different values of *ID* and *LV*. *ID* is the initial density of the simulation, and *LV* defines the limiting velocity above which no vegetation additions are possible. Sparse (pink), channeled (yellow), and filled (green) outcomes are indicated by S, C, and F, respectively. Bold, underlined letters indicate simulations that were run to completion. Plain letters indicate predictions (e.g., if *ID* = 4.3%, *LV* = 0.6 had a filled outcome, cases at the same *LV* and higher *ID* can also be reasonably expected to have a filled outcome). Note that the axes do not have uniform intervals.

landscape, we expect all higher values of *LV* to also produce filled landscapes because the tendency for growth increases with increasing *LV*.

[15] Sparse cases occurred when the modified velocity field did not include regions sufficiently below *LV* to promote growth. In particular, sparse cases were associated with a lack of growth in secondary deposition zones (Fig. 1). This could have been caused by a low *ID* (e.g., <1% for $LV < 0.7$), for which patch spacing was too large to allow lateral interactions (i.e., patch spacing was everywhere greater than the patch interaction length-scale, which was set to *D*), such that no secondary zones occurred. Alternatively, for low values of *LV*, the velocity within the primary and secondary wakes may not have been depressed sufficiently to drop below *LV*, so that there was no growth within the patch wakes. Related to this, the change from sparse to filled outcomes occurred at lower values of *ID* for higher values of *LV*. This makes sense because at higher values of *LV*, the reduction in velocity required to favor growth is smaller, and thus achieved with less vegetation addition. This implies that the value of *ID* leading to full coverage will be dependent on sediment grain size and bare-bed velocity, which set the limiting velocity (*LV*).

[16] If patch–wake interactions were present and provided regions of velocity below *LV*, then the simulation approached either a channeled or filled state. The filled state had a final density near 100% and occurred after the velocity everywhere in the populated zone had dropped below *LV*. A channeled state occurred if the simulation developed a contiguous

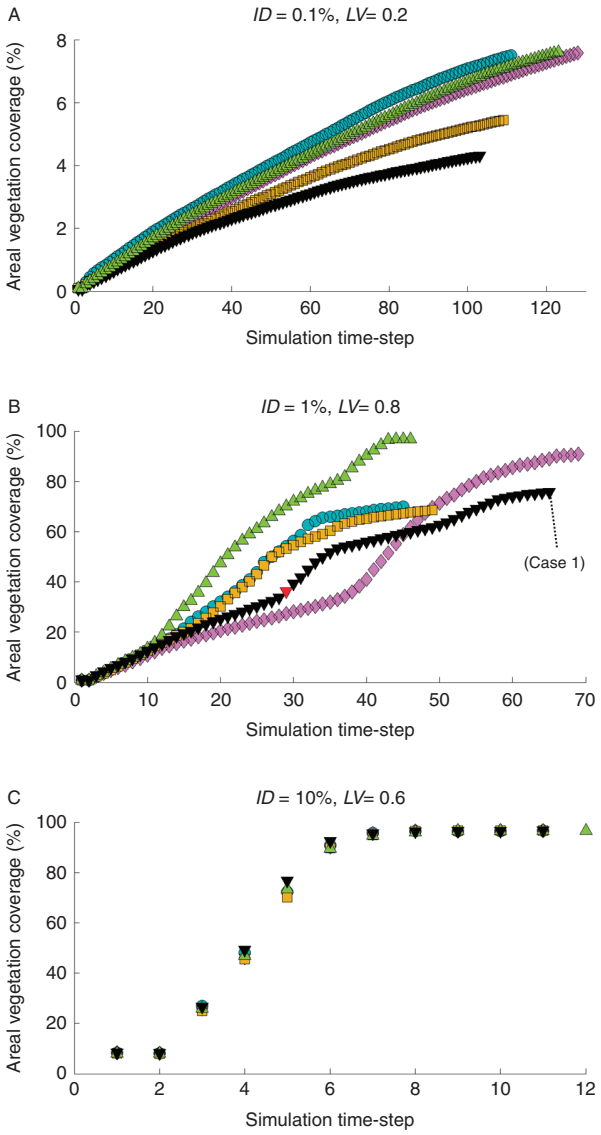

Fig. 6 (A) sparse (*ID* = 0.1%, *LV* = 0.2), (B) channeled (*ID* = 1%, *LV* = 0.8), and (C) filled (*ID* = 10%, *LV* = 0.6) density growth patterns for the same initial conditions under five different random initial patch location configurations, indicated by the five different symbols and colors. *ID* is the initial density of the simulation, and *LV* defines the limiting velocity above which no vegetation additions are possible. The variability among random configurations with the same initial conditions is highest for the channeled case, where different wake effects can lead to a filled case or a channeled case, depending on how quickly the interactions occur. Time-step 29 for Case 1 in (B) is highlighted in red.

region of bare-bed within which the velocity remained sufficiently above *LV* to inhibit plant growth.

[17] The time evolution shown in Fig. 6 provides more detail about how the three landscapes (sparse, channeled, filled, Fig. 4) developed differently. In each case the figure shows five simulations with the same *ID* and *LV*, but with different initial random configurations. For the sparse cases (Fig. 6A), the growth was nearly linear through the entire evolution because no wake interactions occurred. In each time-step, each individual patch added the same area, defined by L_1, producing linear growth. Because the growth was so constrained, the range of final densities, 4.3%–7.6%, was quite small. Channeled cases, in contrast, could take very different development paths depending on the specific initial random configuration, which led to different channel configurations (Fig. 6B). Although all the cases began with the same *ID* (1%), the final area density ranged from 69% to 97% (effectively filled). That both channeled and filled states could result from the same *ID* indicates that the boundary between the channeled and filled states is somewhat blurred; that is, simulations at this boundary have the potential to end as either channeled or filled. Whether a case evolved to channeled or filled depended on whether or not a channel formed early in the simulation. Once formed, a channel could support velocity above *LV*, inhibiting growth and maintaining the channel, even as the vegetation at either side of the channel filled in to 100% coverage. Further, the channeled cases exhibited transitions in growth rate that marked changes in the growth pattern. The shifts were associated with both patch-scale and domain-scale feedbacks (discussed below). Here, we describe the transition associated with patch-scale feedback. The initial random configurations and the probabilistic connection between velocity and vegetation (Fig. 3) created variability in the size of the vegetation clusters and the points in time at which they grew sufficiently large to interact. When the patches grew large enough to interact, the growth rate increased through patch-scale feedback, that is, the formation of secondary deposition zones (Fig. 1) through wake interaction between adjacent patches.

[18] Domain-scale feedbacks were also observed, in which the domain average resistance increased sufficiently to reduce the velocity everywhere below *LV*. For example, consider case 1 in Fig. 6B. There is a sharp change in growth rate near time-step 29, marked in red in Fig. 6B. This shift was associated with the total domain resistance reaching a sufficient level to reduce the velocity everywhere, including the bare regions, to below *LV*, which encouraged vegetation to develop throughout the domain (i.e., a domain-scale feedback), leading to a more rapid rate of growth. The details of this transition are shown in Fig. 7. At time-step 28, previous vegetation additions facilitated by wake interaction, visible by the black sections at the bottom of the domain, had reduced the average velocity in the open, upstream regions of the domain from 0.85 to 0.78, which was below the value of *LV* (0.8). This allowed growth to occur in the bare, upstream regions during time-step 29. Subsequently, these new patches produced growth in their wakes and further lowered the velocity in the open region, such that rapid growth occurred in this section of the flow domain, producing the sudden change in growth rate in Fig. 6B. A similar transition occurred at time-step 39 for the case marked with pink diamond symbols in Fig. 6B.

[19] Finally, a comparison of filled landscapes is shown in Fig. 6C. For *ID* = 10%, patch interaction began after time-step 2, which manifested in the rapid linear growth after this step. All simulations follow the same time evolution, reaching a filled final state after

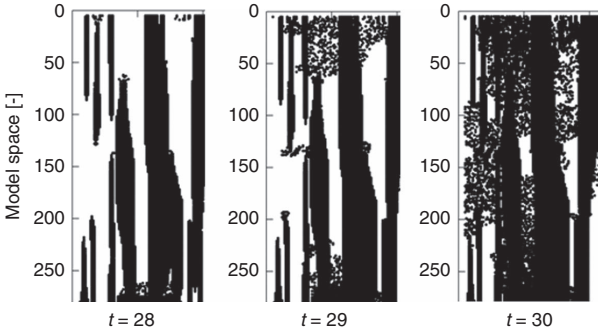

Fig. 7 Vegetation growth in a subsection of the flow domain for case 1 in Fig. 6B. *ID* = 1%, *LV* = 0.8. *ID* is the initial density of the simulation, and *LV* defines the limiting velocity above which no vegetation additions are possible. Vegetation is black and the bare region is white. At time-step 28, the average velocity in the upstream bare region of the domain (rows 5–55) drops from 0.85 to 0.78, which is below *LV*. This produces new growth at the upstream end of the domain in time time-step 29, which in turn accelerates the wake-induced growth observed throughout the domain in time-steps 29 and 30.

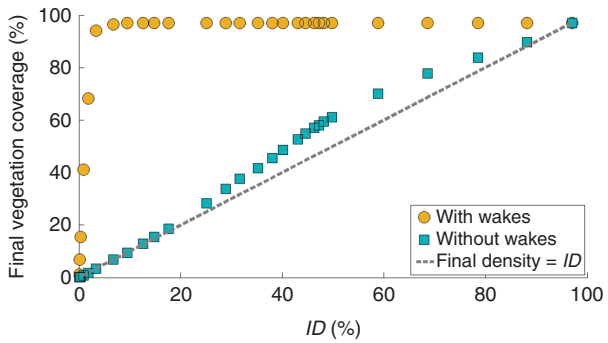

Fig. 8 Final vegetation density as a function of initial vegetation density *ID* at *LV* = 0.5. The final density is always higher when wakes are included. Cases with wakes (yellow circles) reach the same maximum final density for all *ID* > 10%. Cases without wakes (blue squares) do not experience more than a 15% increase in density regardless of *ID* for this *LV*.

just 7 time-steps. Importantly, the model produced filled landscapes for $ID \geq 5.2\%$ for all $LV > 0$ (Fig. 5). This is a promising result for restoration, as it implies that fully covered landscapes can result from fairly sparse initial plantings. As noted above, the formation of channels can inhibit evolution to a filled landscape. The following comparison further illustrates this point. Although cases initiated at $ID = 10\%$ all reached a final state of 100% (Fig. 6C), the cases initiated at $ID = 1\%$, and which all passed through 10% coverage, do not reach 100% (Fig. 6B). This difference was related to the growth pattern that occurred between 1% and 10%, specifically the development of channels. By the time the simulations initiated at 1% passed through 10% coverage, they had already developed channels within which velocity was high enough to suppress vegetation colonization. This made a final state of full coverage (100%) unlikely. In contrast, simulations beginning at a random distribution of 10% did not have preferential channels at this density, and thus had no regions that preferentially maintained sufficiently elevated velocity to exclude vegetation. Instead, the velocity at any location was much closer to the average velocity of the entire simulation. This led to the rapid colonization that resulted in 100% coverage.

[20] To verify the influence of wakes and patch-scale interaction, some cases were run a second time with the wake addition turned off. Significantly different patterns of growth emerged (Figs. 8, 9). In particular, when the wake feature was removed, the final density was often less than that with the wake feature included. For example, for $LV = 0.5$, $ID = 10\%$, the simulation with wakes grew to full coverage, but the simulation without wakes remained at 10% (Fig. 8). The wakes downstream of the patches played a more significant role than the patches themselves in providing positive feedback for growth. In addition, landscape growth was always more rapid with the influence of wakes included (data not shown). The simulations in Fig. 8 were all run with $LV = 0.5$ and different *ID*. At low initial density (0.1%), both simulations remained sparse, and the effect of the wakes was simply to add an isolated zone to each patch that increased the final density by a fixed amount per vegetation patch. As *ID* increased, vegetation patches were eventually close enough to produce patch-scale interaction (i.e., interacting wake zones) and, for the simulations that accounted for this interaction, the final state reached 100% coverage, significantly more than the no-wake cases (Fig. 8).

[21] The impact of varying *LV* at $ID = 1\%$ is shown in Fig. 9. At this *ID*, simulations with wakes reached a final density of ≥35% for any *LV* above 0. For the cases without wakes, between $LV = 0$ and $LV = 0.8$ there was effectively no growth. Without wakes, growth could only be encouraged within one diameter directly upstream and downstream of each patch, or if the domain average velocity drops below *LV*. However, it was only the domain-scale response that led to any significant growth. For example, with $ID = 1\%$, the initial domain-scale velocity was 0.98.

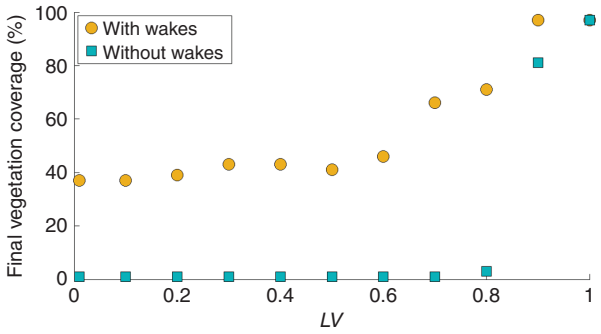

Fig. 9 Final density as a function of limiting velocity *LV*, at fixed initial density, $ID = 1\%$. For simulations with wakes (yellow circles) the final density is always higher than the simulation without wakes (blue squares), except when $LV = 1$ for which all simulations have a final density of 100% (see Fig. 5).

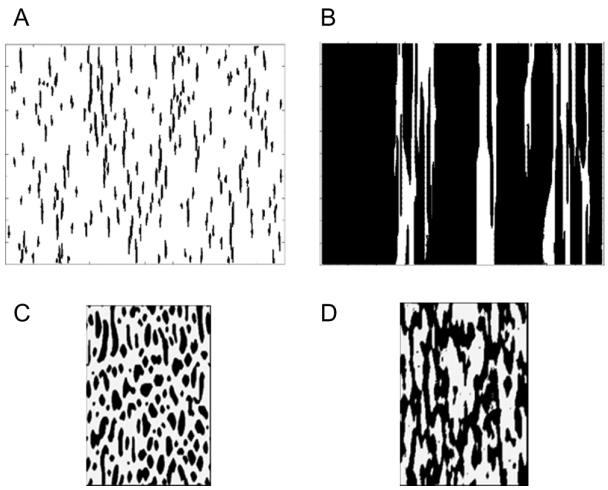

Fig. 10 Comparison of (A) sparse and (B) channeled landscape outcomes to images reported in Larsen and Harvey (2011) as (C) small elongated islands and (D) parallel preferential flow channels. The colors for the images from Larsen and Harvey (2011) have been inverted such that dark indicates vegetation whereas light indicates open channel, consistent with (A) and (B).

Without wakes, the domain average velocity dropped to 0.89 after 27 time-steps. At this point, the scenarios with $LV \geq 0.89$ experienced significant growth through the domain-scale feedback (Fig. 9).

Discussion

[22] There are two scales of feedback that provide positive influences for vegetation development. At the patch scale, low-velocity regions within the wake of individual patches and on the centerline between neighboring patches provide regions favorable to deposition and growth. These wake regions encourage streamwise growth and merger between neighboring patches, which generates lateral growth. At the landscape scale, the addition of vegetation anywhere in the domain is a positive feedback for more development because the addition of any vegetation increases the domain-scale flow resistance, which, for a constant head difference (constant water surface slope), reduces the domain-scale average velocity. If the modeled domain were part of a larger landscape, this process represents the diversion of flow away from a region of higher flow resistance. The reduction of flow over the entire domain raises the probability of vegetation everywhere in the domain. We emphasize that in our model, feedbacks arise purely from differences in hydraulic resistance caused by the presence of the vegetation.

[23] It is interesting to note that our model, which includes a very simple set of flow–vegetation feedbacks, produces landscapes that are similar to those generated in more complex models. Larsen and Harvey (2011) have many processes in their model, including vegetation relationships specific to the Everglades system, explicit calculation of bed shear stresses, rules for differential peat accretion, and nutrient accumulation mechanisms, which together create a diverse set of landscapes. Focusing only on the feedback between flow and hydraulic resistance, our model produced three of the main pattern classes seen in the Larsen and Harvey (2011) model: small elongated islands and parallel preferential flow channels (comparison shown in Fig. 10), as well as many cases that reach full coverage (filled). Similarly, the Larsen and Harvey (2011) model reaches a filled state for 75% of its simulations.

[24] The model also reproduced effects of vegetation growth observed in field studies. The sudden growth transitions observed in Fig. 6B are similar to sudden increases in vegetation growth observed in the field (Gurbisz and Kemp 2014). These authors reconstructed a time series of submerged aquatic vegetation in Chesapeake Bay, which experienced no growth for 16 yr followed by a period of rapid growth for 10 yr. The change in growth was attributed to the vegetation crossing a tipping point associated with a period of drought, which allowed the vegetation in one section to increase above 10%, which subsequently spurred growth throughout the vegetated region. Although not reported, it is probable that the growth above 10% coverage was enough to decrease velocity in the vegetated region to below *LV*, facilitating a positive feedback to growth throughout the vegetated region (i.e., a domain-scale feedback).

[25] The parallel preferential flow channel landscape, characterized by channels separating long, sometimes patchy stands of vegetation, is common to several ecosystems (Temmerman et al. 2007; Larsen and Harvey 2011). In a tidal marsh, Temmerman et al. (2007) observed that channels diverted flow away from vegetated regions, and this encouraged further vegetation development. The channels were distinguished from

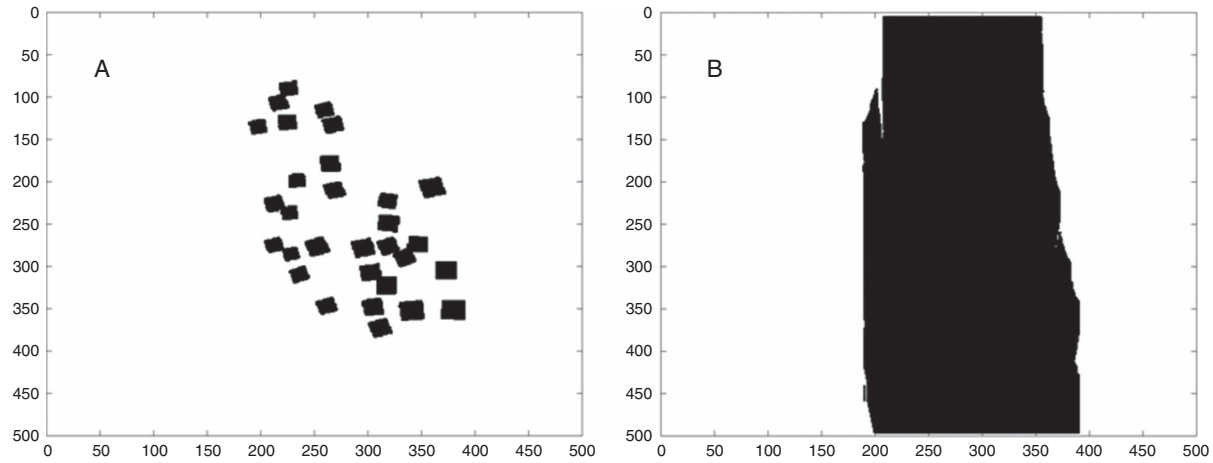

Fig. 11 A — Initial conditions for a simulation representing the planting described in Orth et al. (2010) based on aerial images. The width of the planted region relative to the domain is scaled to match the original field ratio of planting width to channel width. B — Final landscape outcome from the initial conditions in (A) for $LV = 0.7$, where LV defines the limiting velocity above which no vegetation additions are possible.

the vegetated regions by their deeper bathymetry. Indeed, this is the historical definition of a channel. The locally enhanced water depth is the source of the locally lower resistance. Although channels distinguished by differences in depth (cut channels) are common in marsh landscapes, significant channel cutting has not been reported in the literature for seagrass landscapes. However, channels defined simply by a lack of vegetation have been shown to influence seagrass landscape evolution (Luhar et al. 2008). Our study further highlights the fact that the flow-resistance feedback, typically associated with bathymetry, can also be generated by differences in vegetation (bare vs. vegetated). Regions of low-flow resistance (channels) draw flow away from regions of high-flow resistance, producing feedbacks that reinforce the distribution of high- and low-flow resistance. The high flow in channels promotes erosion (further deepening) and inhibits vegetation growth, both of which maintain channels as regions of low-flow resistance. At the same time, the regions of low velocity promote deposition and vegetation growth, both of which maintain the high-flow resistance of these regions.

[26] We consider the role of flow diversion in promoting the success of eelgrass restoration. Between 2004 and 2008, Orth et al. (2010) studied the restoration of eelgrass in one of Virginia's coastal bays. Eelgrass was planted in an array of patches within a section of a tidal channel. The original planting consisted of isolated patches with $ID \approx 4\%$ planted over an area that occupied $\sim$60% of the channel width (Fig. 11). The tidal channel has relatively straight, aligned banks, creating a domain geometry similar to our model. Simulations initiated with the distribution shown in Fig. 11 were run with a range of LV values. The planted region grew to full coverage for cases with $LV \geq 0.7$; that is, the velocity needed to drop below 70% of the bare-bed condition to promote growth. This is a realistic expectation because studies have recorded velocities within seagrass beds that are $<$70% of the adjacent bare-bed value (Fonseca et al. 1982). The evolution to 100% coverage in the planted region occurred in 14 model time-steps. Orth et al. (2010) observed growth to full coverage in 4 yr. This implies that for this system, the time-scale for vegetation–flow feedbacks to manifest, for example, seeds to propagate, establish, and grow to influence flow, or for patches to expand by rhizome growth, is on the order of 3 months. However, we caution that relations between the time in the model and real times will vary based on the biology of the natural system. This restoration case study highlights the positive role of an adjacent bare region, which, like a channel, acts as an attractor for flow, helping to reduce the velocity within the vegetated space, promoting growth and stabilizing the vegetation. This suggests that restoration efforts that intentionally include regions of bare-bed (channels) may be more

successful than those designed with a uniform distribution. Additionally, relying on vegetation-flow feedback to promote growth beyond the initial planting allows the use of fewer initial plants, reducing costs and increasing the feasibility of restoration projects (Orth et al. 2010). Models, such as the one developed in this paper, may provide guidance for which initial density and planting locations will lead to vegetation expansion and stabilization.

[27] Finally, it is important to note the influence of sediment supply, which is revealed by comparing the present model and the Larsen and Harvey (2011) model. The present model is never sediment limited, as deposition and growth are only a function of the velocity field, with no dependence on sediment supply. By excluding the sediment supply limitation, a low-limiting velocity (low *LV*), is associated with lower growth because fewer regions of the domain have velocity below *LV*, which is required for deposition and growth. Similarly, high *LV* is associated with higher growth because there are more regions with velocity less than *LV*, which promotes deposition and growth. From these controls, the present model favors filled landscapes at high values of *LV* (Fig. 5). This result stands in contrast to the Larsen and Harvey (2011) model, which predicts sparse outcomes during conditions of low sediment transport, which would be associated with high *LV*, due to limiting sediment and nutrient fluxes. Further, our growth curve assumes the highest growth at zero velocity, which favors filled landscapes once velocities drop to low levels. This may be unrealistic because very low velocities may lead to nutrient depletion within the meadow, which would then become the limiting factor for growth, that is, consistent with the Larsen and Harvey (2011) model. These contrasting results imply that landscape evolution depends on both the velocity and the sediment supply. The model additionally does not address the possible feedback between the spatial distribution of vegetation and sediment texture, which can influence *LV*. For example, fine materials tend to accumulate within and immediately downstream of vegetated regions, but are removed from regions adjacent to patches, resulting in regions of coarser material (Sand-Jensen and Madsen 1992). Indeed, several factors that are not reflected in the model might impose additional constraints on growth, including wave exposure, nutrient availability, and other factors beyond sediment resuspension that impact light availability. The model reproduced vegetation landscapes without these additional factors because it assumes they are not limiting; however they may still play an important role in the spatial evolution of vegetation.

Significance to Aquatic Environments

[28] This paper presents a simple modeling technique for examining the interaction of flow with patches of vegetation in the evolution of aquatic landscapes. Importantly, it might provide useful information to aquatic restoration efforts, and in particular might guide the selection of initial planting density. The model highlights the role of flow diversion in promoting vegetation growth and landscape evolution at many scales. At the patch scale (i.e., 10s cm), flow diversion reduces the velocity both within the patch and within the wake downstream of the patch, which leads to preferential growth in the streamwise direction. The current model also introduces the possible lateral expansion of patches through the interaction of patch wakes. Comparisons between model runs with and without the patch wakes and wake interaction suggest that this patch-scale feedback has a significant impact on landscape evolution. At larger scales (i.e., 100s cm), flow diversion into channels promotes growth within and stabilizes vegetated regions adjacent to the channel. The current model highlights that a channel can be defined by differences in vegetation cover (bare versus vegetated), in addition to the more traditional definition based on differences in flow depth. Finally, flow diversion at the regional (or modeling domain) scale (i.e., 1000s cm) can encourage growth throughout the domain.

Acknowledgments This material is based upon work supported by the National Science Foundation under grants EAR 0738352. The authors thank Professor Laurel Larsen for guidance in identifying real-world examples of the vegetation regimes.

References

Bentley, I., and H. Karunarathna, 2012. A novel cellular automata approach to estuarine morphodynamic modelling. Coastal Engin. Proc. no. 33. doi:10.9753/icce.v33.sediment.27.

Bouma, T. J., M. Friedrichs, P. Klaassen, B. K. van Wesenbeeck, F. G. Brun, S. Temmerman, M. M. van Katwijk, G. Graf, and P. M. J. Herman. 2009. Effects of shoot stiffness, shoot size and current velocity on scouring sediment from around seedlings and propagules. Mar. Ecol. Prog. Ser. **388**: 293–297. doi:10.3354/meps08130.

Bouma, T. J., L. A. van Duren, S. Temmerman, T. Claverie, A. Blanco-Garcia, T. Ysebaert, and P. M. J. Herman. 2007. Spatial flow and sedimentation patterns within patches of epibenthic structures: Combining field, flume and modelling experiments. Cont. Shelf Res. **27**: 1020–1045. doi:10.1016/j.csr.2005.12.019.

Chen, Z., A. Ortiz, L. Zong, and H. Nepf. 2012. The wake structure behind a porous obstruction and its implications for deposition near a finite patch of emergent vegetation. Water Resour. Res. **48**. doi:10.1029/2012WR012224.

Couwenberg, J. 2005. A simulation model of mire patterning-revisited. Ecography **28**: 653–661.

Duke, N. C., J. O. Meynecke, S. Dittmann, A. M. Ellison, K. Anger, U. Berger, S. Cannicci, K. Diele, K. C. Ewel, C. D. Field, N. Koedam, S. Y. Lee, C. Marchand, I. Nordhaus, and F. Dahdouh-Guebas. 2007. A world without mangroves? Science **317**: 41–42. doi:10.1126/science.317.5834.41b.

Follett, E. M., and H. M. Nepf. 2012. Sediment patterns near a model patch of reedy emergent vegetation. Geomorphology **179**: 141–151.

Fonseca, M. S., J. S. Fisher, J. C. Zieman, and G. W. Thayer. 1982. Influence of the seagrass, *Zostera marina* L., on current flow. Estuar. Coast. Shelf Sci. **15**: 351–364. doi:10.1016/0272-7714(82)90046-4.

Gurbisz, C., and M. Kemp. 2014. Unexpected resurgence of a large submersed plant bed in Chesapeake Bay: analysis of time series data. Limnol. Oceanogr. **59**: 482–494.

Gurnell, A. M., G. E. Petts, D. M. Hannah, B. P. G. Smith, P. J. Edwards, J. Kollmann, J. V. Ward, and K. Tockner. 2001. Riparian vegetation and island formation along the gravel-bed Fiume Tagliamento, Italy. Earth Surf. Process. Landf. **26**: 31–62. doi:10.1002/1096-9837(200101)26:1<31::AID-ESP155>3.0.CO;2-Y.

Gurnell, A. M, K. Tockner, P. Edwards, and G. Petts. 2005. Effects of deposited wood on biocomplexity of river corridors. Front. Ecol. Environ **3**: 377–382. doi:10.1890/1540-9295(2005)003[0377:EODWOB]2.0.CO;2.

Gurnell, A. M., T. D. Blackall, and G. E. Petts. 2008. Characteristics of freshly deposited sand and finer sediments along an island-braided, gravel-bed river: The roles of water, wind and trees. Geomorphology **99**: 254–269. doi:10.1016/j.geomorph.2007.11.009.

Harbaugh, A. 2005. MODFLOW-2005, The U.S. Geological Survey modular ground-water model—the ground-water flow process. U.S. Geological Survey, Techniques and Methods 6-a16 ed. U.S. Geological Survey.

Larsen, L. G., and J. W. Harvey. 2011. Modeling of hydroecological feedbacks predicts distinct classes of landscape pattern, process, and restoration potential in shallow aquatic ecosystems. Geomorphology **126**: 279–296.

Lowe, R. J., U. Shavit, J. L. Falter, J. R. Koseff, and S. G. Monismith. 2008. Modeling flow in coral communities with and without waves: A synthesis of porous media and canopy flow approaches. Limnol. Oceanogr. **53**: 2668–2680. doi:10.4319/lo.2008.53.6.2668.

Luhar, M., J. Rominger, and H. Nepf. 2008. Interaction between flow, transport and vegetation spatial structure. Environ. Fluid Mech. **8**: 423–439. doi:10.1007/s10652-008-9080-9.

Marani, M., E. Belluco, S. Ferrari, S. Silvestri, A. D'Alpaos, S. Lanzoni, A. Feola, and A. Rinaldo. 2006. Analysis, synthesis and modelling of high-resolution observations of salt-marsh eco-geomorphological patterns in the Venice lagoon. Estuar. Coast. Shelf Sci. **69**: 414–426. doi:10.1016/j.ecss.2006.05.021.

Mariotti, G., and S. Fagherazzi. 2010. A numerical model for the coupled long-term evolution of salt marshes and tidal flats. J. Geophys. Res. **115**. doi:10.1029/2009JF001326.

Meire, D., J. Kondziolka, and H. Nepf. 2014. Interaction between neighboring vegetation patches: impact on flow and deposition. Water Resour. Res. **50**. doi:10.1002/2013WR015070.

Orth, R. J., S. R. Marion, K. A. Moore, and D. J. Wilcox. 2010. Eelgrass (*Zostera marina L.*) in the Chesapeake Bay region of mid-Atlantic coast of the U. S. A.: challenges in conservation and restoration. Estuaries Coasts **33**: 139–150. doi:10.1007/s12237-009-9234-0.

Sand-Jensen, K. 1998. Influence of submerged macrophytes on sediment composition and near-bed flow in lowland streams. Freshwater Biol. **39**: 663–679.

Sand-Jensen, K., and T. Vindbaek Madsen. 1992. Patch dynamics of the stream macrophyte, *Callitriche cophocarpa*. Freshw. Biol. **27**: 277–282. doi:10.1111/j.1365-2427.1992.tb00539.x.

Schoelynck, J., T. de Groote, K. Bal, W. Vandenbruwaene, P. Meire, and S. Temmerman. 2012. Self-organised patchiness and scale-dependent bio-geomorphic feedbacks in aquatic river vegetation. Ecography **35**: 760–768. doi:10.1111/j.1600-0587.2011.07177.x.

Scott, J. L., J. M. Friedman, and G. T. Auble. 1996. Fluvial process and the establishment of bottomland trees. Geomorphology **14**: 327–339. doi:10.1016/0169-555X(95)00046-8.

Temmerman, S., T. J. Bouma, J. Van de Koppel, D. Van der Wal, M. B. De Vries, and P. M. J. Herman. 2007. Vegetation causes channel erosion in a tidal landscape. Geology **35**: 631–634. doi:10.1130/G23502A.1.

van Katwijk, M., A. Bos, V. de Jonge, L. Hanssen, D. Hermus, and D. de Jong. 2009. Guidelines for seagrass restoration: importance of habitat selection and donor population, spreading of risks, and ecosystem engineering effects. Mar. Pollut. Bull. **58**: 179–188.

van Wesenbeeck, B. K., J. van de Koppel, P. M. J. Herman, and T. J. Bouma. 2008. Does scale-dependent feedback explain spatial complexity in salt-marsh ecosystems? Oikos **117**: 152–159.

Vandenbruwaene, W., S. Temmerman, T. J. Bouma, P. C. Klaassen, M. B. de Vries, D. P. Callaghan, P. van Steeg, F. Dekker, L. A. van Duren, E. Martini, T. Balke, G. Biermans, J. Schoelynck, and P. Meire. 2011. Flow interaction with dynamic vegetation patches: implications for biogeomorphic evolution of a tidal landscape. J. Geophys. Res: Earth Surface **116**. doi:10.1029/2010jf001788.

Wolters, M., J. Bakker, M. Bertness, R. Jefferies, and I. Moller. 2005. Saltmarsh erosion and restoration in south-east England: squeezing the evidence requires realignment. J. Appl. Ecol. **42**: 844–851. doi:10.1111/j.1365-2664.2005.01080.x.

Zong, L., and H. Nepf 2011. Vortex development behind a finite porous obstruction in a channel. J. Fluid Mech. **691**: 368–391.

Received: 19 May 2014
Amended: 11 August 2014
Accepted: 27 September 2014